Fine structure of the Vavilov-Cherenkov radiation

G. N. Afanasiev,[1] V. G. Kartavenko,[1] and V. P. Zrelov[2]
[1]*Bogoliubov Laboratory of Theoretical Physics, Joint Institute for Nuclear Research, Dubna, Moscow District, Russia*
[2]*Dzhelepov Laboratory of Nuclear Problems, Joint Institute for Nuclear Research, Dubna, Moscow District, Russia*
(Received 21 April 2003; published 17 December 2003)

The aim of this paper is to study the fine structure of the Cherenkov rings. We analyze the experiments performed by one of authors (Zrelov) in which no special focusing devices were used. The broad Cherenkov ring was observed in the plane perpendicular to the motion axis. Using the exact and approximate formulas we investigate how a charge moving uniformly in a medium radiates in a finite space interval (the Tamm problem). The formulas obtained describe the radiation intensity in the whole space, inside and outside the Cherenkov ring. In the plane perpendicular to the motion axis, the radiation fills mainly the finite ring. Its width (proportional to the motion interval) and the energy released in this ring do not depend on the position of the observation plane. Outside the Cherenkov ring, the radiation intensity suddenly drops. Inside it, the radiation intensity exhibits small oscillations which are due to the interference of the Vavilov-Cherenkov radiation and bremsstrahlung. The bursts of the radiation intensity at the ends of the Cherenkov ring are associated with the shock waves arising at the instants when the charge velocity coincides with the light velocity in a medium. For the chosen motion interval, the well-known Tamm formula does not describe the radiation intensity inside the Cherenkov ring for any position of the observation plane. Outside the Cherenkov ring, the Tamm formula is valid only at very large distances. Theoretical calculations are in satisfactory agreement with experimental data. Thus, the combined experimental and theoretical study of the unfocused Cherenkov rings allows one to obtain information on the physical processes accompanying the Cherenkov radiation in the finite spatial interval (bremsstrahlung, transition of the light velocity barrier, etc.).

DOI: 10.1103/PhysRevE.68.066501 PACS number(s): 41.60.Bq, 03.50.De, 13.40.−f

I. INTRODUCTION

The classical Tamm-Frank theory [1] explaining the main properties of the Vavilov-Cherenkov (VC) effect [2,3] is based on the assertion that a charge moving uniformly in a medium with the velocity v greater than the velocity of light c_n in the medium radiates spherical waves from each point of its trajectory [4]. The envelope to these spherical waves propagating with the velocity c_n is the Cherenkov cone with its apex attached to a moving charge and with its normal inclined at the angle θ_c towards the motion axis. Here $\cos\theta_c=1/\beta_n, \beta_n=\beta n, \beta=v/c, c_n=c/n$ (c is the velocity of light in vacuum and n is the medium refractive index).

The radiation of a charge moving uniformly in medium, in a finite space interval, is usually studied in the framework of the so-called Tamm problem [5]. In it, a point charge is at rest at some spatial point up to an instant when it exhibits an instantaneous acceleration acquiring the velocity greater or smaller than c_n. With this velocity a charge moves in some time interval at the end of which it exhibits an instantaneous deceleration coming to the permanent state of rest. Under certain approximations (see below) Tamm obtained the remarkably simple formula which is frequently used by experimentalists to identify the charge velocity [6–8].

Zrelov and Ruzicka [9,10] when analyzing the angular spectrum of the radiation arising in the Tamm problem came to the paradoxical result that this spectrum can be interpreted as an interference of two bremsstrahlung (BS) shock waves arising at the beginning and at the end of the charge motion. There was no room for the Cherenkov radiation in their analysis based on the use of the Tamm approximate formula.

Tamm himself [5] thought that his formula describes both the Cherenkov radiation and bremsstrahlung.

To resolve this controversy, the exact solution of the Tamm problem was obtained and investigated in Ref. [11] (in the time representation for the dispersion-free medium) and in Ref. [12] (in the spectral representation). It was shown there that side by side with BS shock waves, the Cherenkov shock wave (CSW, for short) exists. The results obtained in Refs. [11] and [12] remove the above mentioned inconsistency between Refs. [5] and [9,10] in the following way: Although the Tamm problem describes both the Cherenkov radiation and bremsstrahlung, its approximate solution (i.e., the Tamm formula) does not describe the CSW properly.

We see that due to the approximations involved, an important physics has dropped out from the consideration. It is the goal of this paper to analyze the experimental and theoretical aspects of this new physics. For this we obtain the exact (numerical) and approximate (analytical) theoretical radiation intensities describing a charge motion in finite spatial interval and compare them with existing experimental data. Theoretical intensities (exact and analytical) predict the existence of the CSW of finite extension manifesting as a plateau in the radiation intensity and of the BS shock wave manifesting as the intensity bursts at the ends of this plateau. It turns out that the theoretical (numerical and analytical) and experimental intensities are in satisfactory agreement with each other, but disagree sharply with the Tamm formula. The reasons for this are given in the Discussion section.

According to Ref. [11], when a charge moves in the interval $(-z_0,z_0)$, the CSW is enclosed between the moving charge and the L_1 straight line originating from the $-z_0$ point corresponding to the beginning of motion and inclined at the angle θ_c towards the motion axis. The CSW is perpen-

 ©2003 The American Physical Society

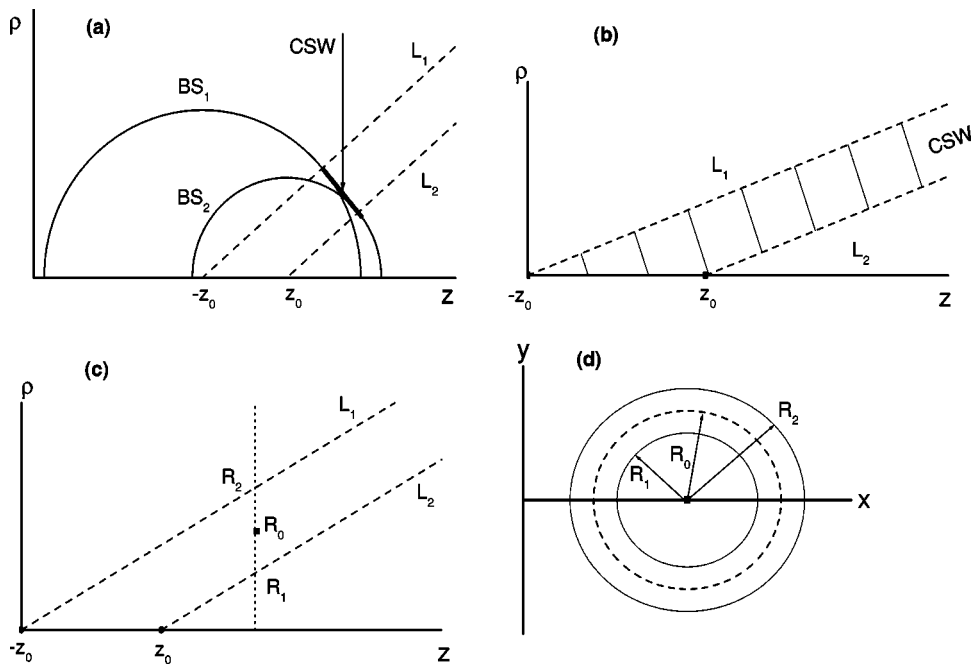

FIG. 1. (a) The position of the CSW and the bremsstrahlung ones arising at the beginning (BS_1) and the end (BS_2) of the charge motion at a fixed instant of time. The CSW is enclosed between L_1 and L_2 straight lines originating from the points corresponding to the boundaries of the motion interval. (b) The propagation of CSW between L_1 and L_2 straight lines. (c) In an arbitrary $z=$const plane perpendicular to the motion axis, the CSW, in the $\phi=$const plane, cuts off the segment of the same length R_2-R_1 for any z. (d) Due to the axial symmetry of the problem, the CSW in the $z=$const plane cuts off the ring with internal and external radii R_1 and R_2, respectively. The width R_2-R_1 of the Cherenkov ring and the energy released in it do not depend on the position z of the observational plane.

dicular to L_1. When a charge stops at the instant t_0, the CSW detaches from it and propagates between the L_1 straight line and the L_2 straight line originating from the z_0 point corresponding to the termination of motion and inclined at the same angle θ_c towards the motion axis.

The positions of BS_1, BS_2 shock waves and the CSW at the fixed instant of time are shown in Fig. 1(a). For an arbitrary instant of time $t>t_0$, the CSW is always tangential to both BS_1 and BS_2 shock waves. The length of CSW (coinciding with the distance between L_1 and L_2) is $L/\beta_n\gamma_n$, where $L=2z_0$ is the motion interval and $\gamma_n=1/\sqrt{|1-\beta_n^2|}$. As time goes, the CSW propagates between L_1 and L_2 with the light velocity in medium c_n [Fig. 1(b)]. The BS_1 and BS_2 shock waves are not shown in this figure.

In the spectral representation (since transition to it involves the time integration) one gets space regions lying to the left of L_1 and to the right of L_2 to which BS_1 and BS_2 shock waves are confined, and the space region between L_1 and L_2 to which BS_1, BS_2, and CSW are confined. Let the measurements of the radiation intensity be made in the plane perpendicular to the motion axis z. Then, CSW cuts out in each of the $z=$const planes the segment of the length $\delta\rho=L/\gamma_n$ independent of z, with its center at $R_0=z/\gamma_n$ [Fig. 1(c)]. This picture refers to a particular $\phi=$const plane (ϕ is the angle in the $z=$const plane). Since the treated problem is the axially symmetrical one, the intersection of the CSW with $z=$const plane looks like a ring with minor and major radii equal to $R_1=R_0-L/2\gamma_n$ and $R_2=R_0+L/2\gamma_n$, respectively [Fig. 1(d)].

This qualitative consideration implies only the possible existence of the Cherenkov ring of finite width. To find the distribution of the radiation intensity within and outside it, the numerical calculations are needed.

When the ratio of the motion interval to the observed wavelength is very large (this is a usual thing in the Cherenkov-like experiments), the Tamm formula has a sharp δ-type peak within the Cherenkov ring. Due to this, it cannot describe a rather uniform distribution of the radiation intensity inside the Cherenkov ring.

It should be mentioned that under the "shock waves" used throughout this paper we do not mean the usual shock waves used; e.g., in acoustics or hydrodynamics where they are the solutions of essentially nonlinear equations. The Maxwell equations describing the charge motion in medium are linear, yet, they can have solutions (when the charge velocity is greater than the light velocity in medium) with properties very similar to the true shock waves. For example, there is no electromagnetic field outside the Cherenkov cone, but an infinite electromagnetic field on its surface and a rather smooth field inside the Cherenkov cone. The analog of the Cherenkov cone in acoustics is the Mach cone.

The observation of the above shock waves encounters certain difficulties when the focusing devices used collect radiation from the part of the charge trajectory lying inside the radiator into the sole ring, thus projecting the VC radiation and bremsstrahlung into the same place. The typical experimental setup with a lens radiator and the corresponding Cherenkov ring are shown in Fig. 2. In its left part, 1 means the proton beam with the energy 657 MeV and diameter 0.5 cm, 2 is the lens radiator with refractive index 1.512, and the

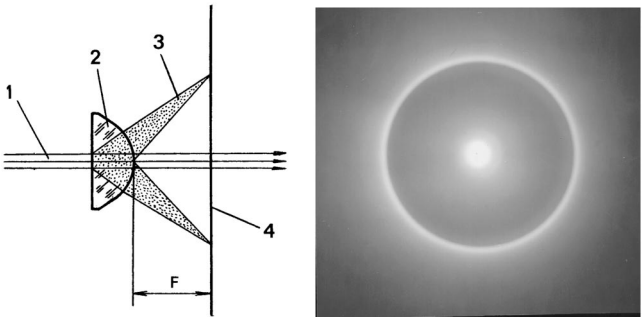

FIG. 2. Left: The scheme of experiment with the lens radiator; 1 is the proton beam, 2 is the lens radiator, 3 is the focused VC radiation, 4 is the plane photofilm placed perpendicularly to the motion axis, and F is the focal distance for paraxial rays; Right: the black-white photoprint from the photofilm shown on the left.

focal distance 2.27 cm (for paraxial rays), 3 is the focused VC radiation ($\theta_{Ch}=35.17°$), and 4 is a plane photofilm (18×24 cm). On the right side there is a black-white photoprint of the photofilm shown on the left. It has the form of a narrow ring.

To see how the VC radiation and bremsstrahlung are distributed in space, we turn to experiments in which the VC radiation was observed without using the focusing devices. These successful (although qualitative) experiments were performed by one of the authors (Zrelov, unpublished) in 1962 when preparing illustrations to monograph [13] devoted to the VC radiation and its applications. In this paper we processed these experimental data. The results are presented in the following section.

One may wonder why we applied the theoretical formalism developed recently to the description of rather old experiments? The reason is that these experiments are the only ones performed without using the special focusing devices and with rather thick dielectric samples.

The plan of our exposition is as follows. The experiments mentioned above are discussed in Sec. II. The main computational formulas (exact and approximate) are collected in Sec. III. The analytic approximate formulas are needed for the qualitative analysis of the exact calculations. Radiation intensities for a number of observation plane positions are presented in Sec IV. In Sec. V, we discuss the results obtained and compare them with experimental data of Sec. II. Section VI contains a brief summary and concrete proposals for the performance of new experiments.

II. SIMPLE EXPERIMENTS WITH 657-MEV PROTONS

A. The first 1962 experiment

The 657-MeV ($\beta=0.808\,75$) proton beam of the phasotron of the JINR Laboratory of Nuclear Problems was used. The experimental setup is shown in Fig. 3. The collimated proton beam (1) with diameter 0.5 cm was directed to the conic polishing plexiglass radiator (2) ($n=1.505$ for $\lambda=4\times 10^{-5}$ cm). The apex angle of 109.7° of the cone enabled the VC radiation (3) to go out from the radiator in the direction perpendicular to the cone surface. The radiation was detected by the plane color 18×24 cm photofilm placed

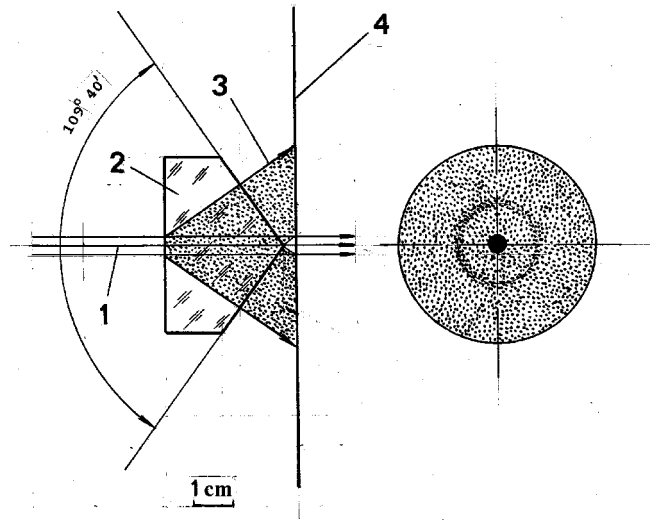

FIG. 3. The experimental setup of the discussed experiment (Zrelov, 1962). The proton beam (1) passing through the conical plexiglass radiator (2) induces the VC radiation (3, shaded region) propagating in the direction perpendicular to the cone surface. The observations are made in the plane photofilm (4) placed perpendicular to the motion axis.

perpendicular to the beam at a distance of 0.3 cm from the cone apex. Nearly 10^{12} protons passed through the conical radiator. The black-white photoprint and the corresponding photometric curve in arbitrary units (from which the beam background was subtracted) are shown in the left and right sides of Fig. 4. The photometric curve describes the distribution $d\mathcal{E}(\rho)/d\rho$ of the energy released inside the ring of the finite width. More accurately, $d\rho\, d\mathcal{E}(\rho)/d\rho$ is the energy released in the elementary ring with minor and major radii ρ and $\rho+d\rho$, respectively. It is seen from this figure that the increment of the radiation intensity takes place at the radius $\rho=2.25$ cm corresponding to the radiation emitted under the Cherenkov angle θ_c from the boundary point where the charge enters into the radiator.

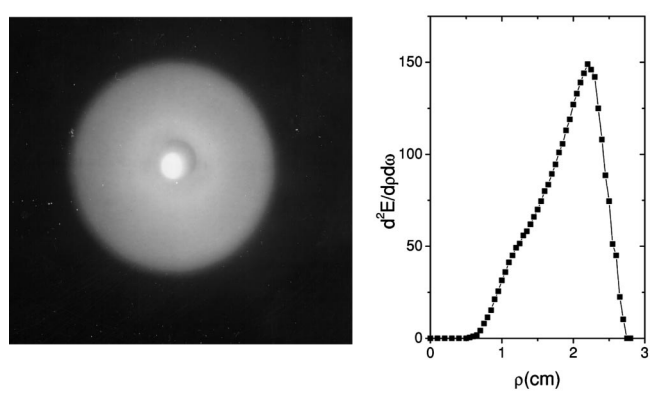

FIG. 4. (Left) The black-white photoprint from the photofilm shown in Fig. 3; (right) The photometric curve (in arbitrary units) corresponding to the left part. One observes the increment of the radiation intensity at $\rho\approx 2.25$ cm which corresponds to the Cherenkov ray emitted from the point where the proton beam enters the radiator.

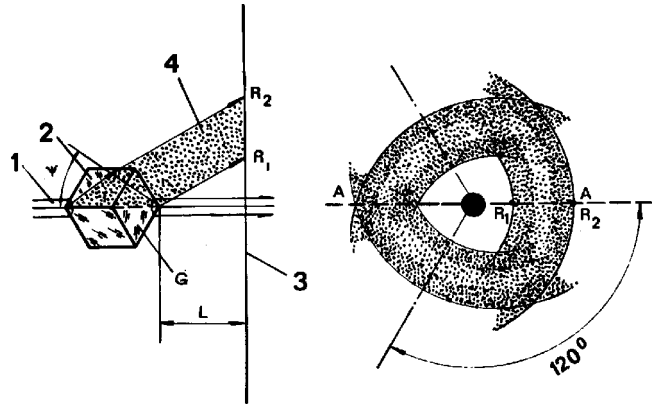

FIG. 5. The experimental setup of another experiment (Zrelov, 1962). The proton beam (1) propagates through the quartz cube (2) along the axis connecting the opposite cube vertices. The observations are made in the plane photofilm (3) placed behind the quartz cube perpendicular to the motion axis; (4) is the direction of the Cherenkov rays passing through one of the cube sides.

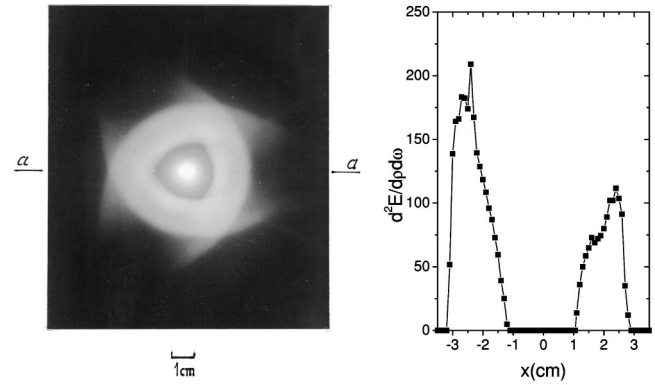

FIG. 6. Left: The black-white photoprint from the photofilm shown in Fig. 5; Right: The photometric curve (in arbitrary units) corresponding to the left part along the direction *a*-*a*; *x* means the distance along *a*-*a*. The increments of the radiation intensity at radii $R_2 \approx 2.3$ cm and $R_1 \approx 1.4$ cm corresponding to the Cherenkov rays emitted at the vertices where the beam enters and leaves the cube, respectively. The radiation intensity for negative *x* describes the superposition of the VC radiation passing through two sides of cube (2). The radiation maxima relating to the ends of the Cherenkov rings are more pronounced than in Fig. 4.

B. The second 1962 experiment

In another experiment performed in the same year (1962), the radiation intensity maxima corresponding to the radiation from the boundary points of the radiator are more pronounced. The experimental setup is shown in Fig. 5.

The radiator was chosen in the form of the crystalline quartz cube of side 1.5 cm. The proton beam (1) passed through the cube (2) along the axis connecting opposite vertices. In this case, the VC radiation went out through the three cube sides inclined at an angle $\psi = 35.26°$ towards the motion axis. Likewise in the first experiment, the plane color photofilm was placed perpendicular to the beam axis, at a distance of $L = 2.35$ cm from the cube vertex. This guaranteed a smaller (as compared with a previous experiment) proton beam background in the VC radiation region. The direction of VC radiation rays (4) through one particular cube side *G* is shown. The black-white photoprint and the corresponding photometric curve (in arbitrary units) measured along the direction "*a*-*a*" (Fig. 5) are shown in Fig. 6. To make the rough estimates, we averaged the crystalline quartz refractive index over ordinary and nonordinary wave vector directions, thus obtaining $n = 1.55$ for $\lambda = 5 \times 10^{-5}$ cm. The corresponding Cherenkov angle was $\theta_c = 37.09°$. In this case, the VC radiation rays emitted from the cube vertices should be at the radii $R_1 \approx 1.4$ cm and $R_2 \approx 2.3$ cm in the photofilm perpendicular to the motion axis. There is a rather pronounced radiation maximum in Fig. 6 only at $R_2 \approx 2.3$ cm.

Theoretical consideration and numerical calculations presented below show that the just mentioned radiation intensity maxima should indeed take place and they are due to the discontinuities at the beginning and the end of the charge motion interval.

III. MAIN COMPUTATIONAL FORMULAS

In the past, the finite width of the Cherenkov rings on the observational sphere *S* of the finite radius *r* was studied analytically and numerically in Ref. [12] in the framework of the Tamm problem. It was shown there that the angular region to which the Cherenkov ring is confined is large for small *r* and diminishes with increase of *r*. However, the width of the band on the observational sphere corresponding to Cherenkov ring remains finite even for infinite values of *r*. Unfortunately, the authors of Ref. [12] were unaware about Zrelov's unpublished experiments discussed above.

Since the measurements in these experiments were made in the plane perpendicular to the motion axis (which we identify with the *z* axis), we should adjust formulas obtained in Ref. [12] to the case treated.

A. The exact formula

In the spectral representation, the nonvanishing *z* component of the vector potential corresponding to the Tamm problem is given [5] by

$$A_z(x,y,z) = \frac{e\mu}{2\pi c}\alpha_T, \tag{3.1}$$

where

$$\alpha_T = \int_{-z_0}^{z_0} \frac{dz'}{R}\exp(i\psi), \quad \psi = k\left(\frac{z'}{\beta} + nR\right),$$

$$R = [\rho^2 + (z-z')^2]^{1/2},$$

$$\rho^2 = x^2 + y^2, \quad k = \frac{\omega}{c}, \tag{3.2}$$

and μ is the magnetic permittivity (in the subsequent concrete calculations we always put $\mu = 1$).

The field strengths corresponding to this vector potential are

$$H_\phi = \frac{ekn\rho}{2\pi c}\int dz' \exp(i\psi)\frac{1}{R^2}\left(-i+\frac{1}{k_n R}\right),$$

$$E_\rho = \frac{iek\mu\rho}{2\pi c}\int dz' \exp(i\psi)\frac{z-z'}{R^3}\left(1+\frac{3i}{k_n R}-\frac{3}{k_n^2 R^2}\right),$$

$$k_n = kn$$

(we do not write out the z component of the electric strength since it does not contribute to the z component of the energy flux which is of interest for us).

The energy flux emitted in the frequency interval $d\omega$ and passing through the circular ring with radii ρ and $\rho+d\rho$ lying in the $z=$const plane is equal to

$$d\omega d\rho \frac{d^2\mathcal{E}}{d\rho d\omega},$$

where

$$\frac{d^2\mathcal{E}}{d\rho d\omega} = 2\pi\rho\frac{c}{2}(E_\rho H_\phi^* + \text{c.c.}) = \frac{e^2k^2n\mu\rho^3}{2\pi c}(I_c I_c' + I_s I_s'). \tag{3.3}$$

Here we put

$$I_c = \int dz' \frac{1}{R^2}\left(\cos\psi_1 - \frac{\sin\psi_1}{k_n R}\right),$$

$$I_c' = \int dz' \frac{z-z'}{R^3}\left[\left(1-\frac{3}{k_n^2R^2}\right)\cos\psi_1 - 3\frac{\sin\psi_1}{k_n R}\right],$$

$$I_s = \int dz' \frac{1}{R^2}\left(\sin\psi_1 + \frac{\cos\psi_1}{k_n R}\right),$$

$$I_s' = \int dz' \frac{z-z'}{R^3}\left[\left(1-\frac{3}{k_n^2R^2}\right)\sin\psi_1 + 3\frac{\cos\psi_1}{k_n R}\right],$$

$$\psi_1 = \frac{kz'}{\beta} + k_n(R-r), \quad r^2 = \rho^2 + z^2. \tag{3.4}$$

B. The Tamm approximate formula

Imposing the conditions (i) $R \gg z_0$ (this means that the observational distance is much larger than the motion interval); (ii) $k_n R \gg 1$, $k_n = \omega/c_n$ (this means that the observations are made in the wave zone); (iii) $nz_0^2/2r\lambda \ll \pi$, $\lambda = 2\pi c/\omega$ (this means that the second-order terms in the expansion of R should be small compared with π since they enter into ψ_1 as a phase; λ is the observed wavelength), Tamm [5] obtained the following expression for the magnetic vector potential:

$$A_z = \frac{e\mu}{\pi n\omega r}\exp(iknr)q,$$

$$q = \frac{1}{1/\beta_n - \cos\theta}\sin\left[\frac{kLn}{2}\left(\frac{1}{\beta_n}-\cos\theta\right)\right]. \tag{3.5}$$

Here $L=2z_0$ is the motion interval and $\beta_n = \beta n$, $\beta = v/c$. Using this vector potential, one easily evaluates the quantity similar to Eq. (3.3)

$$S_z^T = \frac{d^2\mathcal{E}}{d\rho d\omega}(T) = \frac{2e^2\mu z\rho^3}{\pi n c r^5}q^2, \tag{3.6}$$

where $\cos\theta = z/r$ and $r=\sqrt{\rho^2+z^2}$. The value of Eq. (3.6) at $\cos\theta = 1/\beta_n$ is given by

$$(S_z^T)_{\cos\theta=1/\beta_n} = \frac{e^2\mu k^2L^2}{2\pi c n^4\beta^5\gamma_n^3 z}, \quad \gamma_n = \frac{1}{\sqrt{|1-\beta_n^2|}}. \tag{3.7}$$

For large kL, Eq. (3.6) is reduced to

$$(S_z^T)_{kL\gg 1} = \frac{e^2\mu kL}{c}\left(1-\frac{1}{\beta_n^2}\right)\delta\left(\rho - \frac{z}{\gamma_n}\right). \tag{3.8}$$

Integration over ρ gives the energy flux through entire $z=$const plane,

$$\left(\frac{d\mathcal{E}}{d\omega}\right)_{TF} = \frac{e^2\mu kL}{c}\left(1-\frac{1}{\beta_n^2}\right), \quad k = \frac{\omega}{c}, \tag{3.9}$$

which is independent of z and coincides with the Tamm-Frank value [1] (as it should be).

Tamm himself evaluated the energy flux per unit solid angle and per unit frequency through the sphere of the infinite radius r,

$$\left(\frac{d^2\mathcal{E}}{d\Omega d\omega}\right)_T = \frac{e^2\mu}{\pi^2 nc}q^2\sin^2\theta. \tag{3.10}$$

This famous formula obtained by Tamm refers to the spectral representation and is frequently used by experimenters for identification of the charge velocity.

C. The Fresnel approximation

This approximation is valid if the following conditions are satisfied.

(i) The terms of the order L/r and higher are neglected in I, I_c', I_s, and I_s' occurring in Eq. (3.4) if they do not enter the ψ_1 function defined by Eq. (3.4). This approximation, valid if the observational distance r is much larger than the motion interval L, is satisfied in a majority of the Cherenkov-like experiments.

(ii) The terms of the order $1/kr$ and higher are neglected in I, I_c', I_s, and I_s' if they do not enter the ψ_1 function. This approximation, valid if the observational distance r is much larger than the radiated wavelength λ, is also satisfied in a majority of the Cherenkov experiments. For example, $kr = 10^6$ for the typical optical wavelength $\lambda = 6\times 10^{-5}$ cm and the observational distance $r=10$ cm.

(iii) The terms quadratic in z' in the development of R inside ψ_1 defined by Eq. (3.4) are taken into account while the cubic ones are neglected.

Therefore, the conditions for the validity of the Fresnel approximation are

$$\frac{z_0}{r} \ll 1, \quad \frac{\lambda}{r} \ll 1, \quad n z_0^3/(2r^2\lambda) \ll 1.$$

As a result, one obtains

$$I_c = \frac{1}{r^2}\int dz' \cos\psi_1, \quad I_c' = \frac{z}{r^3}\int dz' \cos\psi_1,$$

$$I_s = \frac{1}{r^2}\int dz' \sin\psi_1, \quad I_s' = \frac{z}{r^3}\int dz' \sin\psi_1,$$

$$\frac{d^2\mathcal{E}}{d\rho d\omega} = \frac{e^2 k^2 z n \mu \rho^3}{2\pi c r^5}[(I_1)^2 + (I_2)^2], \tag{3.11}$$

where

$$I_1 = \int dz' \cos\psi_1, \quad I_2 = \int dz' \sin\psi_1,$$

$$\psi_1 = kz'\left(\frac{1}{\beta} - n\cos\theta + \frac{z'}{2r}\sin^2\theta\right).$$

Here θ is polar angle (relative to the motion axis) of the observational point.

The integrals I_1 and I_2 are expressed through the Fresnel integrals. Substituting them into Eq. (3.11) one finds

$$\left(\frac{d^2\mathcal{E}}{d\rho d\omega}\right)_F = \frac{e^2\mu k\rho z}{2cr^2}[(S_+ - S_-)^2 + (C_+ - C_-)^2]. \tag{3.12}$$

Here

$$C_\pm = C(z_\pm), \quad S_\pm = S(z_\pm),$$

$$z_\pm = \sqrt{\frac{k_n r}{2}}\sin\theta\left(\frac{1-\beta_n\cos\theta}{\beta_n\sin^2\theta} \pm \frac{z_0}{r}\right),$$

$C(x)$ and $S(x)$ are the Fresnel integrals defined as

$$S(x) = \sqrt{\frac{2}{\pi}}\int_0^x dt \sin t^2 \quad \text{and} \quad C(x) = \sqrt{\frac{2}{\pi}}\int_0^x dt \cos t^2.$$

From the asymptotic behavior of the Fresnel integrals

$$S(x) \sim \frac{1}{2} - \frac{1}{\sqrt{2\pi}}\frac{\cos x^2}{x}, \quad C(x) \sim \frac{1}{2} + \frac{1}{\sqrt{2\pi}}\frac{\sin x^2}{x}$$

as $x \to \infty$ and their property $C(-x) = -C(x)$, $S(-x) = -S(x)$ it follows that for large kr Eq. (3.12) has a kind of plateau (if $\rho_2 - \rho_1 \ll \rho$)

$$\frac{e^2\mu k\rho z}{cr^2}, \tag{3.13}$$

for $\rho_1 < \rho < \rho_2$, where ρ_1 and ρ_2 are defined by the vanishing of the Fresnel integral arguments. For $r \gg z_0$, they are reduced to

$$\rho_{1,2} = \sqrt{\beta_n^2 - 1}(z \mp z_0).$$

Outside the plateau, for the z fixed and $\rho \to \infty$, Eq. (3.12) decreases like $1/\rho^2$ coinciding with the Tamm formula (3.6). Mathematically, the existence of a plateau is due to the fact that for $\rho_1 < \rho < \rho_2$ the Fresnel integral arguments z_+ and z_- have different signs. At the Cherenkov threshold ($\beta = 1/n$),

$$z_\pm = \sqrt{\frac{k_n r}{2}}\sin\theta\left(\frac{1}{2\cos^2(\theta/2)} \pm \frac{z_0}{r}\right)$$

have the same sign for $r > L$ and the radiation intensity for $kr \gg 1$ and $r > L$ should be small [as compared with the plateau value (3.13)] everywhere.

These asymptotic expressions are not valid at $\rho = \rho_1$ and $\rho = \rho_2$. At these points the radiation intensities are obtained directly from Eq. (3.12),

$$\left(\frac{d^2\mathcal{E}}{d\rho d\omega}\right)_{\rho=\rho_1} = \frac{e^2\mu k z \rho_1}{2cr_1^2}\left\{\left[C\left(\sqrt{\frac{2kn}{r_1}}z_0\sin\theta_1\right)\right]^2 + \left[S\left(\sqrt{\frac{2kn}{r_1}}z_0\sin\theta_1\right)\right]^2\right\},$$

$$\left(\frac{d^2\mathcal{E}}{d\rho d\omega}\right)_{\rho=\rho_2} = \frac{e^2\mu n k z \rho_2}{2cr_2^2}\left\{\left[C\left(\sqrt{\frac{2kn}{r_2}}z_0\sin\theta_2\right)\right]^2 + \left[S\left(\sqrt{\frac{2kn}{r_2}}z_0\sin\theta_2\right)\right]^2\right\}, \tag{3.14}$$

where r_1, r_2, θ_1, and θ_2 are defined as

$$r_1 = \sqrt{\rho_1^2 + z^2}, \quad r_2 = \sqrt{\rho_2^2 + z^2}, \quad \cos\theta_1 = z/r_1,$$

$$\cos\theta_2 = z/r_2.$$

For $kz_0^2/z \gg 1$, one gets

$$\left(\frac{d^2\mathcal{E}}{d\rho d\omega}\right)_{\rho=\rho_1} = \frac{e^2\mu k z \rho_1}{4cr_1^2}, \quad \left(\frac{d^2\mathcal{E}}{d\rho d\omega}\right)_{\rho=\rho_2} = \frac{e^2\mu n k z \rho_2}{4cr_2^2}, \tag{3.15}$$

which is four times smaller than Eq. (3.13) taken at the same points. For $kz_0^2/r \ll 1$, the radiation intensity (3.12) outside the Cherenkov ring coincides with the one given by the Tamm formula (3.6).

1. Frequency distribution

Integrating Eq. (3.13) over ρ from ρ_1 to ρ_2 [suggesting that outside this interval, the radiation intensity (3.12) is negligible], one gets the frequency distribution of the radiated energy,

$$\left(\frac{d\mathcal{E}}{d\omega}\right)_F=\frac{e^2\mu kL}{c}\left(1-\frac{1}{\beta_n^2}\right),\quad k=\frac{\omega}{c}, \tag{3.16}$$

which coincides with the Tamm-Frank frequency distribution (3.9).

2. Energy radiated in the given frequency interval per unit radial distance

Integrating Eq. (3.13) over ω from ω_1 to ω_2, one gets the space distribution of the energy emitted in the frequency interval (ω_1,ω_2). It equals

$$\left(\frac{d\mathcal{E}}{d\rho}\right)_F=\frac{e^2\mu\rho z}{2c^2r^2}(\omega_2^2-\omega_1^2) \tag{3.17}$$

for $\rho_1<\rho<\rho_2$ and zero outside this integral. When performing the ω integration, we disregarded the ω dependence of the refractive index n. This is valid for a rather narrow frequency interval.

3. The total energy radiated in the given frequency interval

Integration of Eq. (3.16) over ω or Eq. (3.17) over ρ gives the total energy emitted in the frequency interval (ω_1,ω_2)

$$\mathcal{E}=\frac{e^2\mu L}{2c^2}(\omega_2^2-\omega_1^2)\left(1-\frac{1}{\beta_n^2}\right). \tag{3.18}$$

(Again, the medium dispersion is neglected.)

D. Quasiclassical (WKB) approximation

To make easier the interpretation of the numerical calculations presented in the following section, we apply the method of the stationary phase for the evaluation of the vector potential (3.1). For $\rho<(z-z_0)/\gamma_n$ and $\rho>(z+z_0)/\gamma_n$ (that is, below L_2 or above L_1) one gets

$$A_z^{BS}=A_1^{BS}-A_2^{BS}, \tag{3.19}$$

where

$$A_1^{BS}=\frac{ie\mu\beta}{2\pi ck}\frac{1}{R_1}\exp(i\psi_1),\quad A_2^{BS}=\frac{ie\mu\beta}{2\pi ck}\frac{1}{R_2}\exp(i\psi_2),$$

$$R_1=\frac{1}{r_1-\beta_n(z+z_0)},\quad R_2=\frac{1}{r_2-\beta_n(z-z_0)},$$

$$\psi_1=k\left(nr_1-\frac{z_0}{\beta}\right),\quad \psi_2=k\left(nr_2+\frac{z_0}{\beta}\right),$$

$$r_1=\sqrt{\rho^2+(z+z_0)^2},\quad r_2=\sqrt{\rho^2+(z-z_0)^2},\quad k=\frac{\omega}{c}.$$

It is seen that if $\beta>1/n$, then A_z^{out} is infinite at $\rho=(z-z_0)/\gamma_n$ and $\rho=(z+z_0)/\gamma_n$, that is, at the border with CSW. There are no singularities in A_z^{out} for $\beta<1/n$. Expanding r_1 and r_2 up to the first order in z_0 ($r_1=r+z_0\cos\theta$, $r_2=r-z_0\cos\theta$), one gets

$$A_z^T=\frac{e\mu q}{\pi cknr}\exp(iknr), \tag{3.20}$$

which coincides with the Tamm vector potential (3.5). Due to the approximations involved, the singularities of A_1^{BS} and A_2^{BS} compensate each other, and the Tamm vector potential (3.20) is finite at all angles. Thus, A_z^{BS} is the quasiclassical analog of the Tamm vector potential.

On the other hand, in the space region $(z-z_0)/\gamma_n<\rho<(z+z_0)/\gamma_n$ (that is, between L_2 and L_1) one has

$$A_z=A_z^{BS}+A_z^{Ch}, \tag{3.21}$$

where A_z^{BS} is the same as in Eq. (3.19) while

$$A_z^{Ch}=\frac{e\mu}{2\pi c}\exp(i\psi_{Ch})\sqrt{\frac{2\pi\beta\gamma_n}{k\rho}}\Theta[\rho-(z-z_0)/\gamma_n]\times\Theta[(z+z_0)/\gamma_n-\rho], \tag{3.22}$$

where $\Theta(x)$ is the step function and

$$\psi_{Ch}=\frac{kz}{\beta}+\frac{\pi}{4}+\frac{k\rho}{\beta\gamma_n}.$$

It should be noted that A_z^{Ch} exists only if $\beta>1/n$. Otherwise ($\beta<1/n$), the vector potential is given by Eq. (3.19) in the whole angular region.

One can ask on what grounds we separated the vector potential into the Cherenkov (A_z^{Ch}) and bremsstrahlung (A_z^{BS}) parts? First, A_1^{BS} and A_2^{BS} exist below and above the Cherenkov threshold while A_z^{Ch} exists only above it. This is what intuitively expected for the VC radiation and bremsstrahlung Second, A_z^{Ch} originates from the stationary point of the integral α_T [see Eq. (3.1)] lying inside the motion interval $(-z_0,z_0)$. For A_1^{BS} and A_2^{BS} the stationary points lie outside this interval, and their values are determined by its boundary ($\pm z_0$) points. Again, this is intuitively expected since the VC radiation is due to the charge radiation in the interval $(-z_0,z_0)$ while the bremsstrahlung is determined by the points ($\mp z_0$) corresponding to the beginning and the end of motion, respectively. Third, to clarify the physical meaning of A_z^{Ch}, we write out the vector potential corresponding to the unbounded charge motion. It equals [4]

$$A_z=\frac{e\mu}{\pi c}\exp\left(\frac{ikz}{\beta}\right)K_0\left(\frac{k\rho}{\beta\gamma_n}\right)$$

for $\beta<1/n$ and

$$A_z=\frac{ie\mu}{2c}\exp\left(\frac{ikz}{\beta}\right)H_0^{(1)}\left(\frac{k\rho}{\beta\gamma_n}\right) \tag{3.23}$$

for $\beta>1/n$. Since this vector potential tends to Eq. (3.22) as $k\rho\to\infty$, A_z^{Ch} entering Eq. (3.21) is a piece of the unbounded vector potential (3.23) confined to the $(z-z_0)/\gamma_n<\rho<(z+z_0)/\gamma_n$ region.

It is seen that for $kr\to\infty$, A_z^{BS} and A_z^{Ch} decrease like $1/kr$ and $1/\sqrt{kr}$, respectively. This means that at large distances, A_z^{Ch} dominates in the $(z-z_0)/\gamma_n<\rho<(z+z_0)/\gamma_n$ region. Thus, A_z has a kind of plateau inside this interval with infinite maxima at its ends (quasiclassical approximation does not work at these points) and sharply decreases outside it. The corresponding quasiclassical field strengths are given by

$$E=E^{BS}+E^{Ch},\quad H=H^{BS}+H^{Ch}, \tag{3.24}$$

$$H^{BS}=H_1^{BS}-H_2^{BS},\quad E^{BS}=E_1^{BS}-E_2^{BS},$$

$$H_1^{BS}=\frac{e\beta\rho}{2\pi ckr_1R_1^2}(k_nR_1+i)\exp(i\psi_1),$$

$$H_2^{BS}=\frac{e\beta\rho}{2\pi ckr_2R_2^2}(k_nR_2+i)\exp(i\psi_2),$$

$$E_1^{BS}=-\frac{e\beta\rho}{2\pi c\epsilon k^2r_1^2R_1^2}\exp(i\psi_1)\times\left[(1-iknr_1)(1-iknR_1)\frac{z+z_0}{r_1}+\frac{r_1}{R_1}\times(2-iknR_1)\left(\frac{z+z_0}{r_1}-\beta_n\right)\right],$$

$$E_2^{BS}=-\frac{e\beta\rho}{2\pi c\epsilon k^2r_2^2R_2^2}\exp(i\psi_2)\times\left[(1-iknr_2)(1-iknR_2)\frac{z-z_0}{r_2}+\frac{r_2}{R_2}\times(2-iknR_2)\left(\frac{z-z_0}{r_2}-\beta_n\right)\right],$$

$$H^{Ch}=-\frac{e}{2\pi c}\sqrt{\frac{2\pi\beta\gamma_n}{k\rho}}\frac{1}{2\rho}\left(\frac{2ik\rho}{\beta\gamma_n}-1\right)\exp(i\psi_{Ch}),$$

$$E^{Ch}=\frac{1}{\epsilon\beta}H^{Ch}.$$

Here ϵ is the electric permittivity ($n^2=\epsilon\mu$). It should be noted that when evaluating field strengths, we did not differentiate step functions entering into Eq. (3.22). If this were done, the δ functions at the ends of the Cherenkov ring appeared. Due to the breaking of the WKB approximation at these points, the vector potentials and field strengths are singular there and the inclusion of the just mentioned δ functions does not change anything. The energy flux along the motion axis is

$$S_z=\left(\frac{d^2\mathcal{E}}{d\rho d\omega}\right)_{WKB}=\pi\rho c(EH^*+HE^*). \tag{3.25}$$

In Eqs. (3.24) and (3.25), $E\equiv E_\rho$ and $H\equiv H_\phi$ (in order not to overload formulas, we dropped the indices of E_ρ and H_ϕ).

We estimate the height of the plateau to which mainly H^{Ch} and E^{Ch} contribute. It is given by

$$S_z|_{plateau}=\pi\rho c[E^{Ch}(H^{Ch})^*+H^{Ch}(E^{Ch})^*]\approx\frac{e^2\mu k}{c\beta_n^2\gamma_n}. \tag{3.26}$$

Since S_z is negligible outside this plateau and since infinities at the ends of the Cherenkov ring are unphysical (they are due to the failure of the WKB method at these points) the frequency distribution is obtained by multiplying Eq. (3.26) by the width of the Cherenkov ring,

$$\left(\frac{d\mathcal{E}}{d\omega}\right)_{WKB}=\frac{e^2k\mu}{c\beta_n^2\gamma_n}\frac{L}{\gamma_n}=\frac{e^2\mu kL}{c}\left(1-\frac{1}{\beta_n^2}\right). \tag{3.27}$$

This coincides with the Tamm-Frank formula (3.9). It is rather surprising that quite different angular distributions corresponding to the Tamm intensity (3.6), to the Fresnel one (3.12), and the quasiclassical one (3.25) give the same frequency distribution (3.9).

IV. NUMERICAL RESULTS

In Fig. 7, the radiation intensities are presented for various distances δz of the observation plane (δz is the distance from $z=z_0$ point corresponding to the termination of motion). We observe the qualitative agreement of the exact radiation intensity (3.3) with the Fresnel one (3.12). Both of them sharply disagree with the Tamm intensity (3.6) which does not contain the CSW responsible for the appearance of plateau in Eqs. (3.3) and (3.11). Figure 7(d) demonstrates that at large observation distances ($\delta z=100$ cm) the Tamm radiation intensity approaches the exact one outside the Cherenkov ring .

In Fig. 8, the magnified versions of exact radiation intensities corresponding to $\delta z=0.3$ cm and $\delta z=1$ cm are presented. In accordance with quasiclassical predictions, one sees the maxima at the ends of the $(z-z_0)/\gamma_n<\rho<(z+z_0)/\gamma_n$ interval. In Sec. I the special optical devices focusing the rays directed under the Cherenkov angle into one ring was mentioned. In the case treated, it is the plateau shown in Figs. 7 and 8 and the BS peaks at its ends that are focused into this ring. The remaining part of BS will form the tails of the focused total radiation intensity. Probably, for such compressed radiation distribution the Tamm formula has a greater range of applicability.

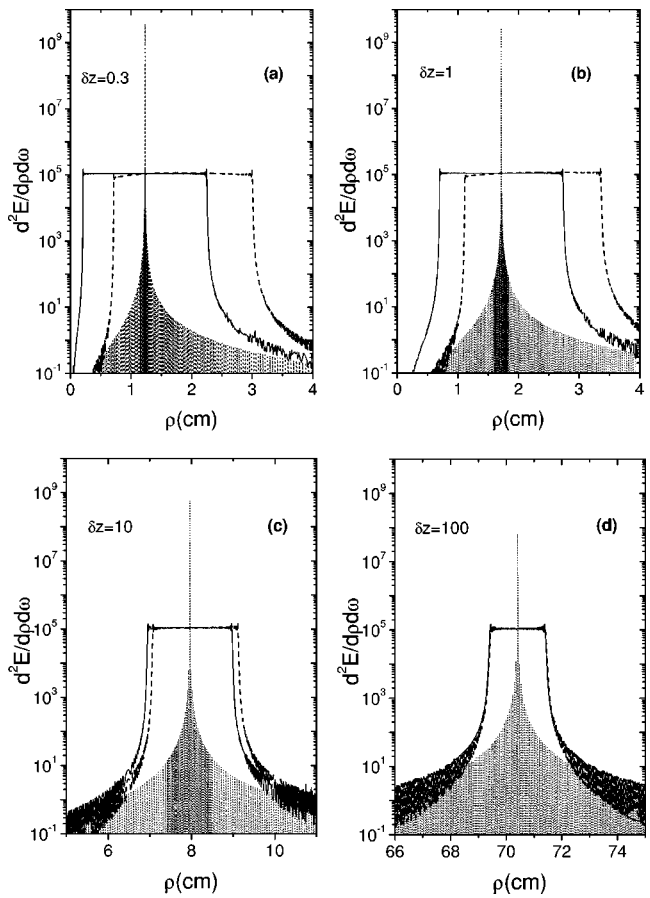

FIG. 7. Theoretical radiation intensities in a number of planes perpendicular to the motion axis for the experimental setup shown in Fig. 3; δz means the distance (in cm) from the cone vertex to the observation plane. The solid, dashed, and dotted curves refer to the exact, Fresnel, and Tamm intensities. In this figure and the following ones, the theoretical radiation intensities are in e^2/cz_0 units.

V. DISCUSSION

A. Vavilov-Cherenkov radiation and bremsstrahlung on the sphere

In the original and in nearly all subsequent publications on the Tamm problem, the radiation intensity was considered on the surface of the sphere of the radius r much larger than the motion interval $L=2z_0$. It is easy to check that on the surface of the sphere of the finite radius r, the intervals

$$\rho>(z+z_0)/\gamma_n, \quad (z-z_0)/\gamma_n<\rho<(z+z_0)/\gamma_n,$$

and

$$\rho<(z-z_0)/\gamma_n$$

correspond to the angular intervals

$$\theta>\theta_1, \quad \theta_2<\theta<\theta_1, \quad \text{and} \quad \theta<\theta_2,$$

where θ_1 and θ_2 are defined by

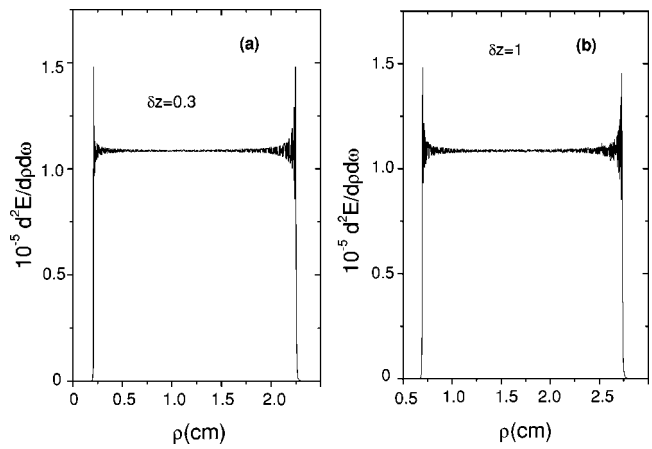

FIG. 8. Exact theoretical radiation intensities in the $\delta z=0.3$ cm and $\delta z=1$ cm planes.

$$\cos\theta_1=-\frac{\epsilon_0}{\beta_n^2\gamma_n^2}+\frac{1}{\beta_n}\left[1-\left(\frac{\epsilon_0}{\beta_n\gamma_n}\right)^2\right]^{1/2}$$

and

$$\cos\theta_2=\frac{\epsilon_0}{\beta_n^2\gamma_n^2}+\frac{1}{\beta_n}\left[1-\left(\frac{\epsilon_0}{\beta_n\gamma_n}\right)^2\right]^{1/2}. \tag{5.1}$$

Here $\epsilon_0=z_0/r$. For $r\gg z_0$,

$$\theta_1=\theta_c+\frac{\epsilon_0}{\beta_n\gamma_n}, \quad \theta_2=\theta_c-\frac{\epsilon_0}{\beta_n\gamma_n},$$

where θ_c is defined by $\cos\theta_c=1/\beta n$. In this case, the Tamm formula (3.10) is valid for $\theta<\theta_2$ and $\theta>\theta_1$, that is, nearly in the whole angular region. It should be added that the existence of the Cherenkov shock wave on the sphere is masked by the smallness of the angular region to which it is confined. It seems at first that on the observation sphere of infinite radius there is no room for CSW. This is not so. Although $\Delta\theta=\theta_1-\theta_2=2\epsilon_0/\beta_n\gamma_n$ is very small for $r\gg z_0$, the length of an arc corresponding to $\Delta\theta$ in a particular $\phi=$const plane of the sphere S is finite: it is given by $\mathcal{L}=2z_0/\beta_n\gamma_n$ and does not depend on the sphere of radius r (for $r\gg z_0$). Due to the axial symmetry of the problem, on the observation sphere S, the region to which the VC radiation is confined looks like a band of the finite width $\mathcal{L}$. Thus, the observation of the Cherenkov ring on the sphere is possible if the detector dimensions are much smaller than $\mathcal{L}$.

B. Vavilov-Cherenkov radiation and bremsstrahlung in the plane perpendicular to the motion axis

More pronounced the separation of the VC radiation and the BS looks in the plane perpendicular to the motion axis. We illustrate this using the quasiclassical intensities as an example. In Fig. 9(a), we present the quasi-classical intensity (3.25) for $\delta z=0.3$ cm. We observe perfect agreement be-

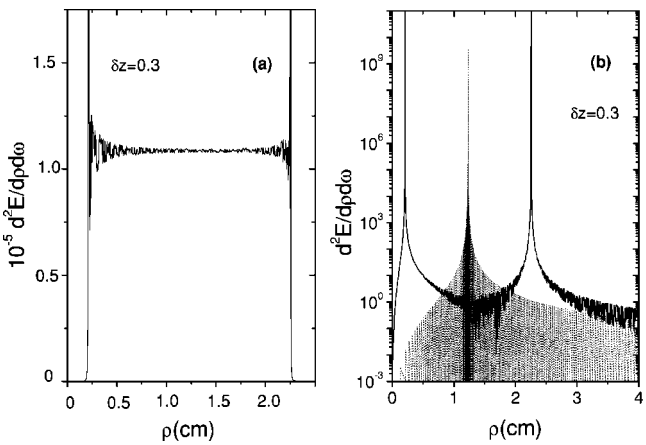

FIG. 9. (a) Quasiclassical radiation intensity in the $\delta z = 0.3$ cm plane. It coincides with the exact one shown in Fig. 8(a) everywhere except for the boundary points of the Cherenkov ring where the quasiclassical intensities are infinite due to the breaking of the WKB approximation. (b) The quasiclassical bremsstrahlung intensity (solid curve) and the Tamm one (dotted curve) in the $\delta z = 0.3$ cm plane. The sharp disagreement between them is observed.

tween it and the exact one shown in Fig. 8(a) everywhere except for the boundaries of the region to which the VC radiation is confined. The quasi-classical approximation is unique in the sense that contributions of the VC radiation and the BS are clearly separated in the vector potential (3.21) and field strengths (3.24). To see the contribution of the BS, we omit A_z^{Ch}, E^{Ch}, and H^{Ch} in these relations by putting them to zero. The resulting intensity describing BS is shown in Fig. 9(b). It sharply disagrees with the Tamm intensity (3.6). From the smallness of the BS intensity everywhere except for the boundaries of the Cherenkov ring it follows that oscillations of the total radiation intensity inside the Cherenkov ring are due to the interference of the VC radiation and the BS.

C. On the nature of the bremsstrahlung shock waves in the Tamm problem

Some words should be added on the nature of BS shock waves discussed above. In Refs. [9,10] they were associated with velocity jumps at the beginning and the end of motion. On the other hand, the smoothed Tamm problem was considered in Ref. [14] in the time representation. In it, the charge velocity v changes smoothly from zero up to some value $v_0 > c_n$ with which it moves in some time interval. Later, v decreases smoothly from v_0 to zero. It was shown in Ref. [14] that at the instant when v coincides with the light velocity in a medium c_n, a complex arises consisting of the CSW with its apex attached to a moving charge, and the shock wave SW_1 closing the Cherenkov cone (and not coinciding with shock wave originating at the beginning of motion). The inclination angle of the normal to SW_1 towards the motion axis (defining the direction in which SW_1 radiates) changes smoothly from 0 at the motion axis up to the Cherenkov angle θ_c at the point where SW_1 intersects the Cherenkov cone. Therefore, the radiation produced by the SW_1 fills the angular region $0 < \theta < \theta_c$. As time goes, the dimensions of the above complex grow since its apex moves with the velocity $v > c_n$, while the shock wave SW_1 propagates with the velocity c_n. In the past, on the existence of radiation arising at the Cherenkov threshold was suggested on the purely intuitive grounds in [15].

Since in the original Tamm problem the charge velocity changes instantly from 0 to v_0, the shock waves are in fact a mixture of these *three shock waves* having zero dimensions at the initial instant of time. Due to the specificity of the Tamm problem, the CSW and SW_1 are not separated in subsequent instants of time too. They are marked as CSW in Fig. 1(a) and 1(b). The smoothed Tamm problem was also considered in the last part of Ref. [11] in the spectral representation. It was shown there that when a motion length along which a charge moves nonuniformly tends to zero, its contribution to the total radiation intensity also tends to zero. There are no velocity jumps for the smoothed problem and, therefore, the BS cannot be associated with instantaneous velocity jumps. However, there are acceleration jumps at the beginning and the end of motion and at the instants when the accelerated motion meets the uniform one. Thus, BS can still be associated with acceleration jumps. To clarify the situation, the Tamm problem with absolutely continuous charge motion (for which the velocity itself and all its time derivatives are absolutely continuous functions of time) was considered in [16]. It was shown there that a rather slow decrease in the radiation intensity outside the above plateau is replaced by the exponential damping (in the past, for the charge motion in vacuum, the exponential damping for all angles was recognized in Ref. [17]). It follows from this that the authors [9,10] were not entirely wrong if under the BS shock waves used by them, one understands the mixture of three shock waves mentioned above and originating from the jumps of velocity, acceleration, other higher velocity time derivatives, and from the transition of the medium light velocity barrier.

This is also confirmed by the consideration of radiation intensities for various charge velocities. Figure 10(a) demonstrates that the position of the radiation intensity maximum approaches the motion axis, while its width diminishes as the charge velocity approaches the Cherenkov threshold ($\beta = 1/n \approx 0.665$). The radiation intensities presented in Fig. 10(b) show their behavior just above ($\beta = 0.67$) and below ($\beta = 0.66$) the Cherenkov threshold. It is seen that the maxima of the underthreshold and the overthreshold intensities differ by 10^5 times. Far from the maximum position, they approach each other. The radiation intensity at the Cherenkov threshold shown in Fig. 10(c) is three orders smaller than the one corresponding to $\beta = 0.67$. The calculations in Figs. 10(a–c) were performed using the Fresnel approximate intensity (3.12) which is in good agreement with the exact one (3.3) for the treated position ($\delta z = 10$ cm) of the observational plane (as Fig. 7 demonstrates).

To see manifestly how the bremsstrahlung changes when one passes through the Cherenkov threshold, we present in Fig. 10(d) the quasiclassical radiation BS intensities evaluated for $\beta = 0.67$ [in this case the VC radiation was removed by hand from (3.24) similarly as it was done in Fig. 9(b)] and $\beta = 0.66$. The position of the observational plane is (δz

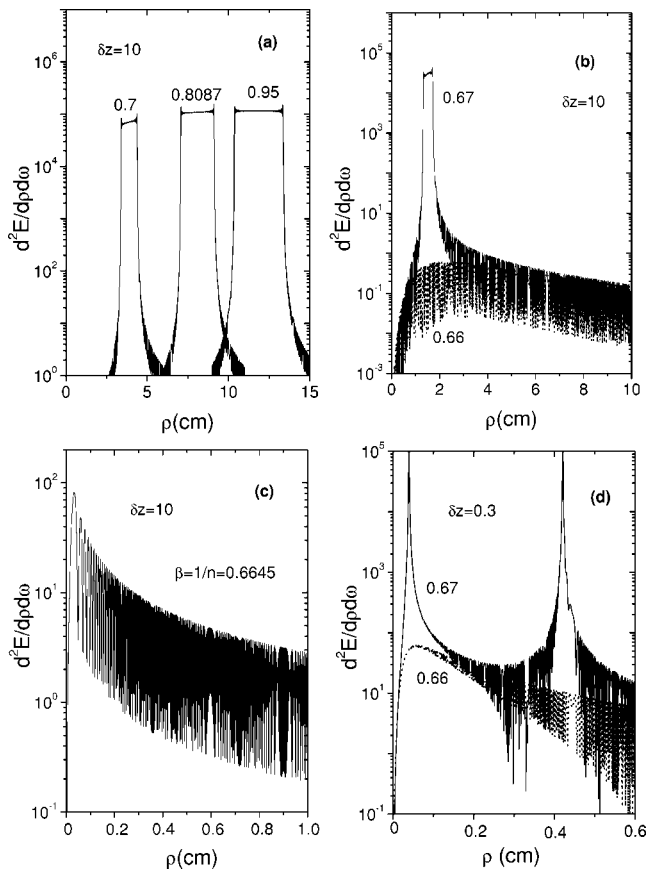

FIG. 10. (a) Radiation intensities for a number of charge velocities above the Cherenkov threshold in the $\delta z = 10$ cm plane. As the charge velocity approaches the light velocity in medium, the position of the Cherenkov ring approaches the motion axis while its width diminishes. (b) Radiation intensities for the charge velocity slightly above and below the Cherenkov threshold in the $\delta z = 10$ cm plane. (c) Radiation intensity at the Cherenkov threshold in the $\delta z = 10$ cm plane. In accordance with theoretical predictions (see Sec. III C) it is much smaller than above the threshold; (d) Quasiclassical BS intensities for the charge velocity slightly above and below the Cherenkov threshold in the $\delta z = 0.3$ cm plane.

$=0.3$ cm). Again, we observe the sharp decrease in the BS intensities in the neighborhood of their maxima when one passes the Cherenkov barrier. This confirms that the BS shock waves used in Refs. [9,10] are the mixture of three shock waves mentioned above for the charge velocity above the Cherenkov threshold. For the charge velocity below the Cherenkov threshold, only the BS shock waves originating from the jumps of velocity, acceleration, and other higher velocity time derivatives survive. They are much smaller than the singular shock wave originating when the charge velocity coincides with the medium light velocity.

D. Comparison with experiment

Strictly speaking, the formulas obtained above and describing the fine structure of the Cherenkov rings are valid if the observations are made in the same medium where a charge moves. Because of this, the plateau of the radiation intensity and its bursts at the ends of this plateau cannot be associated with the transition radiation which appears when a charge intersects the boundary between two media. Turning to the comparison with an experiment, we observe that it corresponds to the charge moving subsequently in air, in medium, and, finally, again in air. The transition radiation [18,19] arising at the boundary of medium with air is approximately 100 times smaller than the VC radiation [20,21]. Since the uniformly moving charge does not radiate in air where $\beta n < 1$ and radiates in medium where $\beta n > 1$, the observer inside the medium associates the radiation with instantaneous appearance and disappearance of a charge at the medium boundaries and with its uniform motion inside the medium. We quote, e.g., Jelly (Ref. [22], p. 59): "A situation alternative to that of a particle of constant velocity traversing a finite slab may arise in the following way; suppose instead that we have an infinite medium and that a charged particle, initially at rest at a point A, is rapidly accelerated up to a constant velocity (above the Cherenkov threshold) which it maintains until, at a point B, it is brought abruptly to rest. If, as in the first case, the distance $AB = d$, the output of Cherenkov radiation will be the same as before. In this case, there will be radiation at the two points A and B; this will be now identified as a form of acceleration radiation. This and transition radiation are essentially the same; the intensities work out the same in both cases and it is only convention which decides which term shall be used." This justifies the applicability of the Tamm problem for the description of the discussed experiments.

Comparing theoretical intensities with the experimental ones we see the following: (i) theoretical intensities have a plateau (Figs. 7–10), while the experimental ones have a triangle form (Figs. 4 and 6); (ii) the observed radiation peaks at the boundaries of the Cherenkov rings are not so pronounced as the predicted ones.

Probably, the triangle form of the observed radiation intensities is due to the smooth change of the charge velocity inside the dielectric. For such a motion, the radiation intensities obtained in Refs. [11,12,16] had indeed a triangle form. We estimate now the energy losses for the experiment treated. For the protons with energy 657 MeV, the energy ionization losses in plexiglass with density $\rho = 1.2$ g/cm^3 are $\Delta E/\Delta z = 2.91$ MeV/cm [23]. This gives $\Delta E = 8.58$ MeV for the radiator length 2.95 cm. The corresponding proton velocity change is $\Delta\beta = 2.3\times 10^{-3}$. Alternatively, it can be associated with a smooth change of the refractive index at the border of vacuum and dielectric.

The item (ii) can be understood if one takes into account that experiments mentioned in Sec. II were performed with a relatively broad proton beam (0.5 cm in diameter). This leads to the smoothing of the boundary peaks after averaging over the proton beam diameter.

VI. CONCLUSION

According to quantum theory [24], a charge uniformly moving in medium with the velocity greater than the light velocity in medium radiates γ quanta at the angle θ_c towards the motion axis ($\cos\theta_c = 1/\beta n$). It should be noted that for the uniform charge motion in unbounded medium, a photo-

plate placed perpendicular to the motion axis will be darkened with the intensity proportional to $1/\rho$ (ρ is the distance from the motion axis) without any maximum at the Cherenkov angle. Despite its increase for small ρ, the energy emitted in a particular ring with the width $d\rho$ is independent of ρ. The surface of the cylinder coaxial with the motion axis will be uniformly darkened.

The Cherenkov ring can be observed only for the finite motion interval. In the $z=\text{const}$ plane, the ring width is proportional to the charge motion interval L: $\Delta R = L/\gamma_n$ ($\gamma_n = 1/\sqrt{|1-\beta_n^2|}$, $\beta_n = \beta n$). It does not depend on the position z of the observation plane. The frequency dependence enters only through the refractive index n. The radiation emitted into a particular ring does not depend on z. For the fixed observation plane, the radiation intensity oscillates within the Cherenkov ring. These oscillations are due to the interference of bremsstrahlung and the Vavilov-Cherenkov radiation in Eq. (3.24). The large characteristic peaks at the ends of the Cherenkov ring are due to the bremsstrahlung shock waves which include shock waves originating from the jumps of velocity, acceleration, other higher velocity time derivatives, and from the transition of the medium light velocity barrier. The finite width of the Cherenkov ring in the $z=\text{const}$ plane is due to the Cherenkov shock wave. Inside the Cherenkov ring ($R_1 < \rho < R_2$), the Tamm formula does not describes the radiation intensity at any position of the observation plane (see Fig. 7). Outside the Cherenkov ring ($\rho < R_1$ and $\rho > R_2$), the exact radiation intensity and the one given by the Tamm formula are rather small. In this angular region they approach each other at large distances satisfying $kz_0^2/r \ll 1$. For the experiments treated in the text, the left hand side of this inequality equals unity at the distance $r \approx 1$ km. On the other hand, the exact formula (3.3) describes the radiation intensity in all space regions.

We conclude that the experiments performed with a relatively broad 657 MeV proton beam passing through various radiators point to the existence of diffused radiation peaks at the boundary of the broad Cherenkov rings. This supports theoretical predictions [9,10,14] on the existence of the shock waves arising when the charge motion begins and when the charge velocity coincides with the medium light velocity.

It is desirable to repeat experiments similar to those described in Sec. II with the charged particle beam of a smaller diameter (≈ 0.1 cm), with a rather thick dielectric sample, without using the focusing devices and for various observation distances. This should result in appearance of more pronounced, just mentioned, radiation peaks.

[1] I.E. Tamm and I.M. Frank, Dokl. Akad. Nauk SSSR **14**, 107 (1937).
[2] P.A. Cherenkov, Dokl. Akad. Nauk SSSR **2**, 451 (1934).
[3] S.I. Vavilov, Dokl. Akad. Nauk SSSR **2**, 457 (1934).
[4] I.M. Frank, *Vavilov-Cherenkov Radiation* (Nauka, Moscow, 1988).
[5] I.E. Tamm, J. Phys. (USSR) **1**, 439 (1939).
[6] J.D. Lawson, Philos. Mag. **45**, 836 (1954).
[7] J.D. Lawson, Am. J. Phys. **33**, 1002 (1966).
[8] D.K. Aitken, R.E. Jennings, A.S.L. Parsons, and R.N.F. Walker, Proc. Phys. Soc. London **82**, 710 (1963).
[9] V.P. Zrelov and J. Ruzicka, Czech. J. Phys., Sect. B **39**, 368 (1989).
[10] V.P. Zrelov and J. Ruzicka, Czech. J. Phys. **42**, 45 (1992).
[11] G.N. Afanasiev, Kh. Beshtoev, and Yu.P. Stepanovsky, Helv. Phys. Acta **69**, 111 (1996); G.N. Afanasiev, V.G. Kartavenko, and Yu.P. Stepanovsky, J. Phys. D **32**, 2029 (1999); G.N. Afanasiev and V.M. Shilov, *ibid.* **35**, 854 (2002).
[12] G.N. Afanasiev, V.G. Kartavenko, and J. Ruzicka, J. Phys. A **33**, 7585 (2000); G.N. Afanasiev and V.M. Shilov, J. Phys. D **33**, 2931 (2000).
[13] V.P. Zrelov, *Vavilov-Cherenkov Radiation in High-Energy Physics* (Israel Program for Scientific Translations, Jerusalem, 1970)
[14] G.N. Afanasiev, S.M. Eliseev, and Yu.P. Stepanovsky, Proc. R. Soc. London, Ser. A **454**, 1049 (1998); G.N. Afanasiev and V.G. Kartavenko, Can. J. Phys. **77**, 561 (1999); G.N. Afanasiev and V.M. Shilov, Phys. Scr. **62**, 326 (2000).
[15] A.A. Tyapkin, JINR Rapid Commun. **3[60]-93**, 26 (1993); V.P. Zrelov, J. Ruzicka, and A.A. Tyapkin, *ibid.* **1[87]-98**, 23 (1998).
[16] G.N. Afanasiev, V.M. Shilov, and Yu.P. Stepanovsky, Nuovo Cimento Soc. Ital. Fis., B **117B**, 815 (2002).
[17] I.I. Abbasov, Sov. Phys.–Lebedev Inst. Rep. No. **1**, 31 (1982); No. 18, 25 (1985); I.I. Abbasov, B.M. Bolotovskii, and V.A. Davydov, Usp. Fiz. Nauk **149**, 709 (1986); [Sov. Phys. Usp. **29**, 788 (1986)]; B.M. Bolotovskii and V.A. Davydov, Izv. Vuzov, Radiofizika **1**, 31 (1981).
[18] V.L. Ginzburg and I.M. Frank, Zh. Eksp. Teor. Fiz. **16**, 15 (1946).
[19] V.L. Ginzburg and V.N. Tsytovich, *Transition Radiation and Transition Scattering* (Hilger, London, 1990).
[20] J. Ruzicka and V.P. Zrelov, Nucl. Instrum. Methods **165**, 307 (1979).
[21] A. Hrmo and J. Ruzicka, Nucl. Instrum. Methods Phys. Res. A **451**, 506 (2000).
[22] J. V. Jelley, *Cerenkov Radiation and its Applications* (Pergamon Press, London, 1958).
[23] J.F. Janni, At. Data Nucl. Data Tables **27**, 284 (1982).
[24] V.L. Ginzburg, Zh. Eksp. Teor. Fiz. **10**, 589 (1940).